CHAPTER 5

Hydrologic Cycle Climate Research

The Earth's atmosphere is unique amongst the known planetary atmospheres in that it possesses a complete hydrologic cycle. That is, we find water in its three phases: gaseous, as water vapor; liquid, as cloud liquid water; and solid, as ice and snow. The existence of a complete hydrologic cycle on the Earth greatly modifies the climate, making this planet hospitable to a wide variety of life. It, however, also greatly complicates understanding and prediction of climate because the water and energy cycles interact in a non-linear way on all time and space scales. On the shortest time scales, within thunderstorms, the three phases of water can be found at the same time within a vertical column in the atmosphere. On seasonal to interannual time scales, the effects of regional changes in sea surface temperature in the Pacific Ocean are communicated globally by changes in the tropical atmospheric hydrologic cycle. On decadal to centennial time scales, differences in precipitation minus evaporation drive the global oceanic thermohaline circulation thought by many to be the Achilles heel of long term climate variability. Thus, hydrologic cycle climate research truly cuts across all of the NOAA Strategic Plan themes and provides the link between these themes and human dimensions.

5.1. Using satellite data for climate studies

The complex process of using satellite data for climate applications is illustrated schematically in **Fig. 5.1**. The ultimate goal of this process is to better understand the satellite data and then apply this knowledge to process studies of climate applications leading to improved predictions. There are two paths to reaching this goal, the forward problem and the inverse problem. In the forward problem, sample geophysical variables are run through a forward radiative transfer model, along with specific information about the satellite instrument such as the instrumental error characteristics and spectral response functions, and the outputs are simulated radiances. This process gives us an idea of what performance we might anticipate from a given instrument. The inverse problem begins with the actual satellite observations. These observations are then used in an inverse radiative transfer model to produce retrievals of geophysical variables. In this process, additional constraints are often applied to the satellite observations such as use of a forecast first guess, other *a priori* data such as clustered radiosonde observations, and radiance bias corrections. Observed radiances are compared to simulated radiances and retrieved geophysical variables are compared to observed geophysical variables and the totality of this knowledge is then applied to process studies of climate applications.

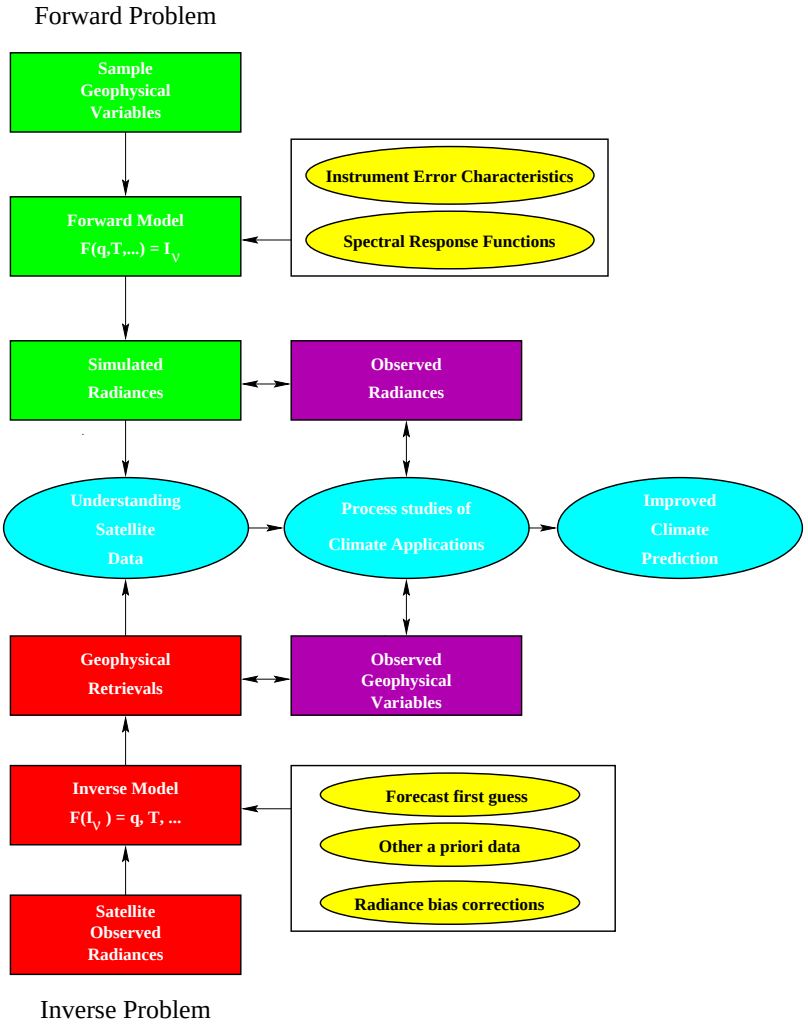

Fig. 5.1. Schematic of the forward and inverse radiative transfer processes as applied to the use of satellite observations for climate monitoring and prediction.

5.2. Satellite error characteristics - A key issue for climate studies

A variety of methods are required to characterize the errors from any satellite observational system. These include, but are not limited to, forward radiative transfer simulation studies, on-board calibration, vicarious calibration and validation with in-situ observations, random and systematic sampling errors, and retrieval errors. A complete discussion of the error characteristics applied to HIRS channel 12 observations can be found in Wu et al. (1993) and Bates et al. (1996). The typical lifetime of a satellite instrument is on the order of 3-5 years. Obtaining a long time series of observations from satellites requires the use of many similar, but slightly differ-

ent instruments, on many different satellites. Thus, a key issue for the use of satellite data in climate studies is the accurate characterization of instrument errors from one instrument to the next. Bates et al. (1996) have established a method for the intersatellite calibration of NOAA polar-orbiting satellite HIRS/MSU instruments. **Fig. 5.2** shows the empirical distribution functions of HIRS channel 12 brightness temperature anomalies for the overlap periods of different NOAA satellites from 1979-1995. There are four lines on each diagram; one for each satellite and one for the ascending and descending passes from each satellite. Generally, there is little difference between the ascending and descending passes from a single instrument, but there are sometimes significant differences between satellites. This suggests that differences in the relative filter response functions between the different satellites are the largest source of discrepancy between the different satellites. To obtain a seamless time

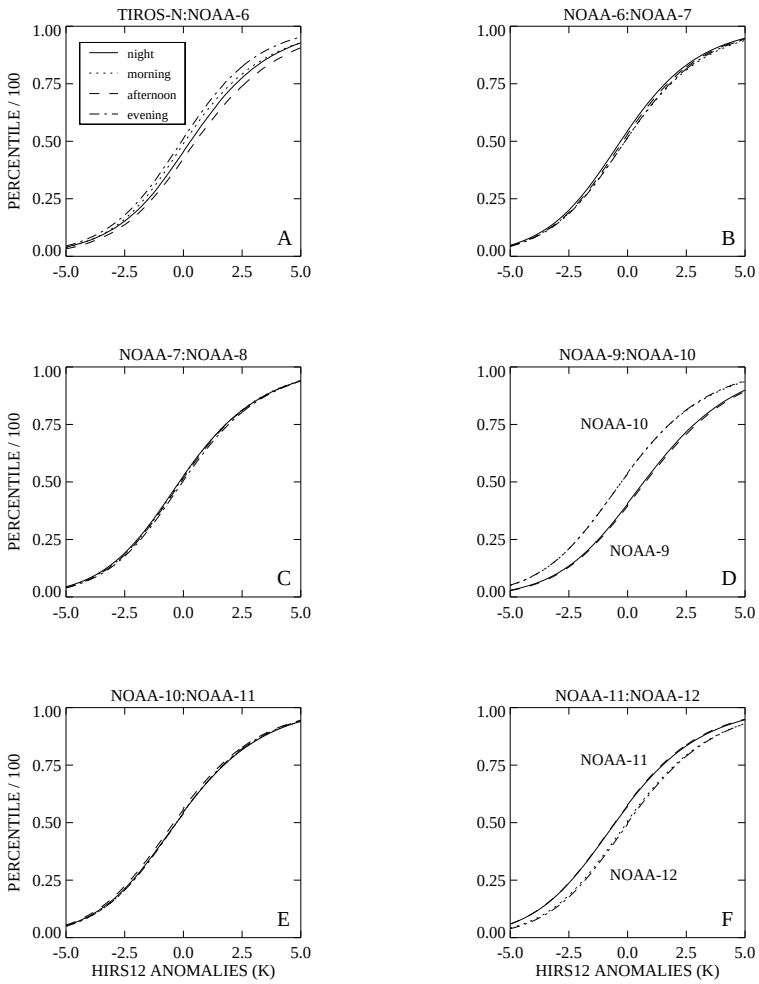

Fig. 5.2. Empirical distribution functions of overlaps between operational satellites used for intercalibration of HIRS channel 12 upper tropospheric water vapor channels.

series of these observations, all anomaly distributions are adjusted to a baseline instrument. To date, we have only analyzed the NESDIS cloud cleared radiances, but we are now re-examining raw level 1b data as part of the TOVS Pathfinder program.

5.3. Global studies of the atmospheric hydrologic cycle

5.3.1. Interannual variability of upper tropospheric humidity

Empirical orthogonal function (EOF) analysis was performed separately on the HIRS 12 upper tropospheric humidity (UTH), Reynolds blended SST, and all-sky outgoing longwave radiation (OLR) monthly mean anomaly datasets. To keep the comparisons uniform, the data were analyzed from 1982-1993 (since the satellite SST data only begin in 1982) for the tropical region 30˚N-30˚S. In all cases, the first mode is associated with interannual, global variability during ENSO warm events. Because of this, the principle component time series for each dataset has been plotted on a single figure (**Fig. 5.3d**). The amount of variance explained by the first mode ranges from 12% for the HIRS 12 UTH, to 24% for the OLR, and to 32% for the SST. All the correlations are significant at the 99% level assuming only 72 degrees of freedom (half the total number of months). Correlations are quite high between OLR, HIRS12 and the SST anomalies (.86 and .78) but the highest correlations are found between the OLR and HIRS12 (.93).

The spatial patterns of the leading mode for each parameter are shown in **Fig. 5.3a-c**. The classic ENSO warm event SST signature (**Fig. 5.3a**) is evident with positive anomalies in the central and eastern equatorial Pacific and negative anomalies in the western equatorial Pacific extending poleward to the extratropics. This interannual SST EOF pattern has been found in independent analysis of ship-only data and satellite-only data (Bates, 1994). The spatial pattern for OLR anomalies (**Fig. 5.3b**) shows a pattern of near equatorial anomalies that results from the shift of convection from the western Pacific Ocean to the central and eastern Pacific during warm events. There are positive OLR anomalies centered near the dateline and extending into the eastern equatorial Pacific. Negative OLR anomalies are found in the western equatorial Pacific and there is a small negative anomaly over northeastern Brazil.

The spatial pattern of the UTH EOF (**Fig. 5.3c**) shows some similar features, but also some distinctly different features when compared to the OLR. Along the equator in the Pacific Ocean, the UTH and OLR features are most similar. At the equator and the dateline, there is a minimum in UTH. The minimum extends eastward to a second minimum in the eastern Pacific. Relative maxima along the equator are found in the western Pacific and across South America extending over northeast Brazil. The most striking difference between the UTH and OLR, however, occurs in the subtropical latitudes. A large maximum in UTH is found just southeast of Hawaii. There is only a weak hint of this anomaly in the OLR data. The UTH data also show a series of maxima and minima across the southern hemisphere subtropics includ-

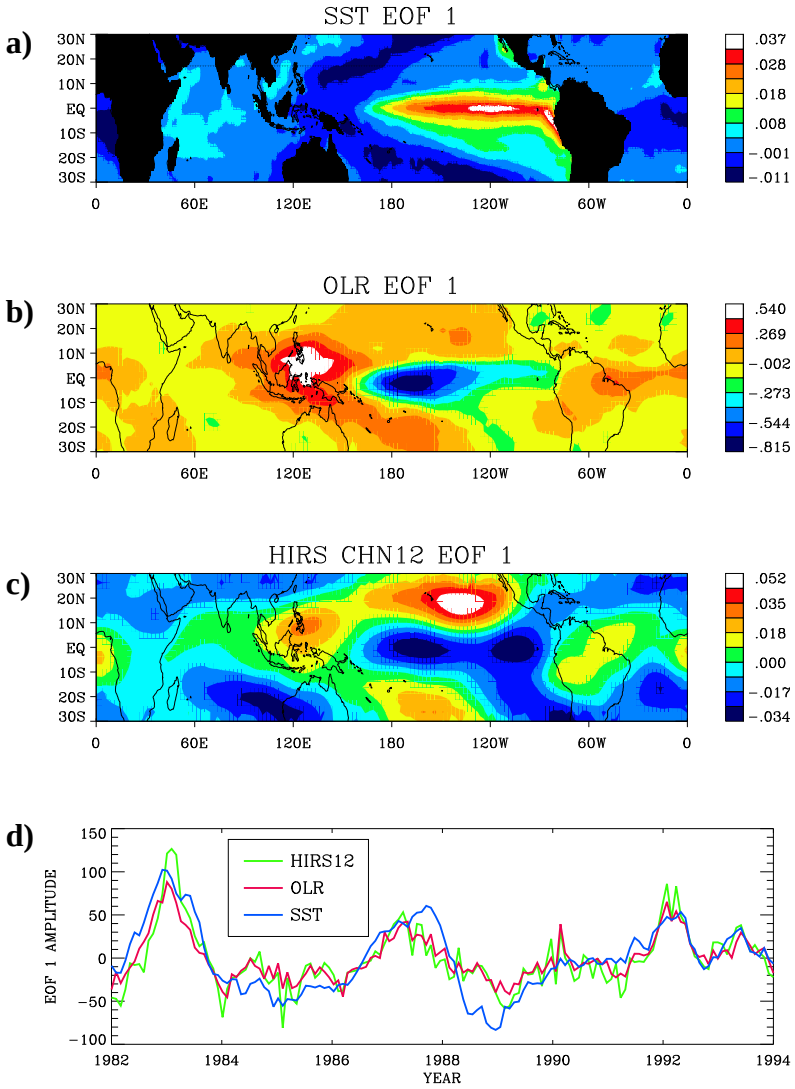

Fig. 5.3. Spatial pattern of leading mode interannual empirical orthogonal function for a) Reynolds I/O sea surface temperature anomalies, b) outgoing longwave radiation anomalies, c) HIRS12 water vapor brightness temperature anomalies, and d) time series of leading mode empirical orthogonal function for Reynolds I/O sea surface temperature anomalies (˚C, dashed line), outgoing longwave radiation anomalies (W m^{-2}, dotted line), and HIRS12 upper tropospheric humidity (%, solid line).

ing a minimum from southwestern Australia extending westward towards Madagascar, a maximum to the east of Australia, and two minima further east one on either side of South America.

An examination of the tropical area average interannual changes in SST, UTH, and Tropospheric temperature (MSU2), however, shows no significant correlation between UTH and SST and MSU2 time series (**Fig. 5.4**). The behavior of tropical UTH appears quite different from one ENSO event to the other. During the 1982-83 ENSO the UTH decreases markedly, during the 1986-87

ENSO event the UTH remains about constant, and during the 1991-92 ENSO the UTH increases slightly. The most striking aspect of these time series is the dramatic drop in tropical UTH during the 1982-83 ENSO. This suggests that a negative UTH feedback does exist for certain states of the tropical hydrologic cycle. We are continuing our analysis of these data sets and collaborating with GCM model runs to improve our understanding of these variations.

5.3.2. Precipitation estimates from satellite microwave and infrared observations

Precipitation plays a crucial role in the Earth's global climate system, especially in the tropics where the resulting release of latent heat is the main source of energy for driving large-scale atmospheric motions. Because very little in-situ data is available over many regions, satellite remote sensing is the only realistic way of providing global rainfall estimates for climate research. The advent of satellite passive microwave technology, which has the ability to see beyond the cloud tops viewed by visible and infrared sensors, has provided new prospects for global rainfall estimation. Passive microwave data provides a more physically direct relationship between rainfall and the observed brightness temperatures than infrared or visible retrieval techniques. Precipitation can be detected either through the emission of thermal energy associated with absorption by liquid raindrops over a cold background such as the ocean or through scattering by frozen hydromete-

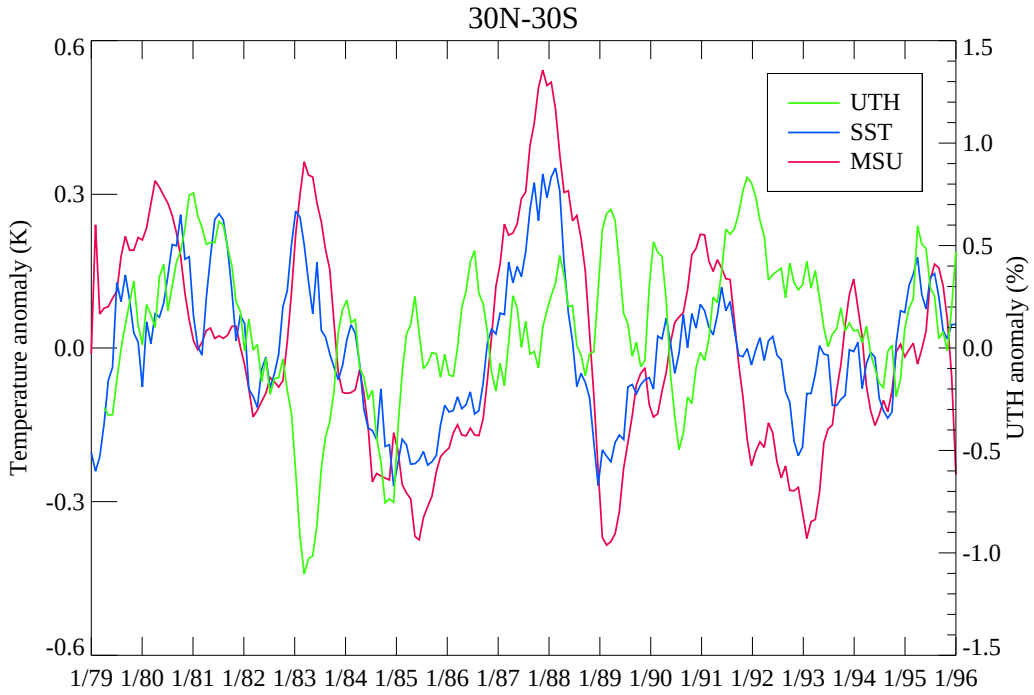

Fig. 5.4. Monthly mean interannual anomalies of SST, UTH, and Tropospheric temperature (MSU2).

ors in upper cloud regions. Although the scattering approach is less direct, it can be used to infer rainfall rates over land regions where emission techniques do not work.

Berg and Chase (1992) computed a climatology of monthly rainfall estimates over the tropical Pacific using passive microwave satellite observations from the special sensor microwave/imager (SSMI) for the period July 1987 through December 1991. An initial analysis of this data by Berg and Avery (1994) found that the major precipitation features as well as the seasonal variability of the rainfall distributions were in good agreement with expected values, while the moderately intense 1986-87 El Niño and the intense La Niña during 1988-89 accounted for significant interannual variability during this time period. A comparison of the SSMI estimates with other satellite retrieval techniques for April 1988 is shown in **Fig. 5.5**. This figure shows the problems with the infrared techniques (OLR and GPI) in discriminating status clouds from light rainfall as well as difficulty in detecting shallow convection in the central Pacific ITCZ region. The large variability in the SSMI estimates is also evident, indicative of the limited sampling of a single polar orbiting satellite.

A detailed analysis of the errors associated with the monthly SSMI rainfall estimates by Berg and Avery (1995) found that the limited sampling by the polar-orbiting defense meteorological satellite program (DMSP) spacecraft is the dominant source of error in the monthly values. To address this problem, Berg (1994) calibrated high spatial and temporal resolution infrared observations from geostationary satellites using the SSMI microwave retrievals. A comparison of results using this approach during TOGA-COARE with other satellite retrieval algorithms as part of the third Global Precipitation Climatology Project (GPCP) algorithm intercomparison project indicates improved climatological estimates over techniques using either the SSMI passive microwave or infrared observations alone. Involvement with a total of six satellite rainfall intercomparison projects through both the GPCP and NASA's WetNet Project have led to significant improvements in operational rainfall algorithms (Berg et al., 1997) as well as a better understanding of global rainfall variability and the problems associated with detecting and estimating rainfall intensity.

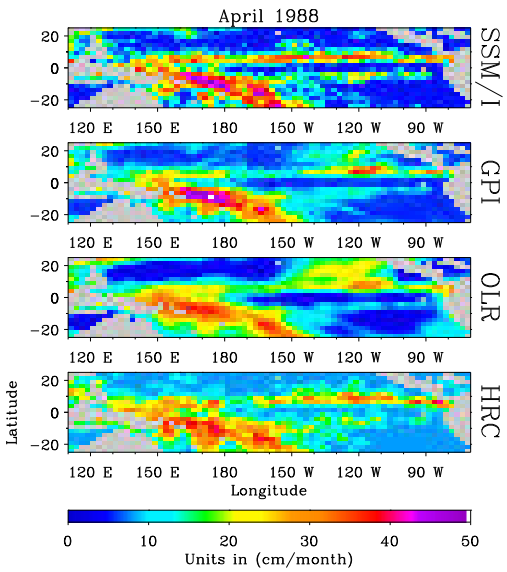

Fig. 5.5. A comparison of the monthly rainfall for April 1988 estimated from SSMI (Berg and Chase, 1992), the outgoing longwave radiation (OLR), Arkin and Meisner's [*Mon. Wea. Rev.*, **115**, 297(1987)] GPI technique, and the highly reflective cloud (HRC) index by Kilonsky and Ramage [*J. Appl. Meteor.*, **15**, 972(1976)].

5.4. Process studies of the atmospheric hydrologic cycle

5.4.1. The East Asian monsoon

Studies based on coupled ocean-atmosphere models and observations have shown that there exists a "predictability barrier" for the ENSO-like variations in the Eastern Asia monsoon region in boreal spring. In the study of the climatology of the South China Sea monsoon, we found that the seasonal transition in the northern hemisphere starts with the summer monsoon onset in the South China Sea (SCS) region. The timing of the SCS onset, however, is strongly dependent on different time-scale systems not only from the tropics, such as the tropical disturbances and the ITCZ in the western Pacific, intraseasonal oscillations and monsoon depressions from the Indian ocean and the ENSO events, but also from the subtropical region such as the western Pacific subtropical high (WPSH). Moreover, seasonal and interannual variations of the sea surface temperature in the Pacific and South China Sea also contribute to the development of the large-scale thermodynamic instability over the SCS. Therefore, we believe that to overcome the "predictability barrier", the models must correctly describe mechanisms of the above systems, and particularly, their interaction processes.

Many previous studies on the Asian monsoon focused on the role of the deep convection, in particular the role of the ITCZ, on monsoon onset. Studies on the interannual and intraseasonal variations of the western Pacific subtropical high, unfortunately, are few because of lack of observations in this region, especially for the study of hydrological processes. Recently, we have used the UTH data to examine normal, early, and delayed monsoon onset years in the SCS region (**Fig. 5.6**) during 1979 - 1995. During a normal onset year, we find weak anomalies of UTH throughout the global tropics. The early monsoon onset year of 1984 is characterized by strong negative UTH anomalies in the central equatorial Pacific and positive UTH anomalies in the western Pacific. The late monsoon onset of 1993 is similar to the normal monsoon onset except for a tendency for slightly stronger positive UTH anomalies in the SCS. We are continuing to explore the use of UTH data as a predictor of SCS monsoon onset.

5.4.2. Pan American climate studies

Understanding the role of hydrological processes, and rainfall in particular, on short-term climate variability in the Pan American regions is critical to improving models and subsequent climate prediction efforts. Due to the lack of in-situ observations over the east Pacific, however, the hydrology of this region and the dynamics involving the transport of moisture between the east Pacific and the Americas is poorly understood. Our knowledge of rainfall processes over the Americas, particularly with regard to the monsoons, and the impact these processes have on hydrologic and energy balances throughout the Pan American region suffers from a number of deficiencies. A comparison of annual average rainfall from several satellite retrieval techniques is shown in **Fig. 5.7**, which demonstrates the poor agreement between these different techniques along the east Pacific ITCZ. Based on NMC model analysis, Janowiak et al.

[*18th Climate Diagnostics Workshop*, NOAA, 216(1993)] suggested that this discrepancy is the result of shallow convection in this region, resulting in warmer cloud tops in the IR and thus less rainfall estimated by the GPI technique. This hypothesis, however, does not explain differences between the two microwave emission retrieval schemes from SSMI and MSU. A pilot field observation program is planned over the east Pacific intertropical convergence zone for September 1997. Continually updated climatologies of satellite precipitation, water vapor, and other cloud properties (Berg and Avery, 1994) provide the large-scale context for studying the dynamics of this region and the resulting interactions with hydrological processes over the continents.

Berg (1994) has shown that for precipitating clouds (as determined from SSMI), the ratio of cloud top temperatures below 235 K, which is the cutoff used by the GPI retrieval technique, to the total is much greater over the west Pacific warm pool region than over the east Pacific. In the warm pool region this ratio is close to 60%, while the value is closer to 20% over the east Pacific. As a result, infrared-based satel-

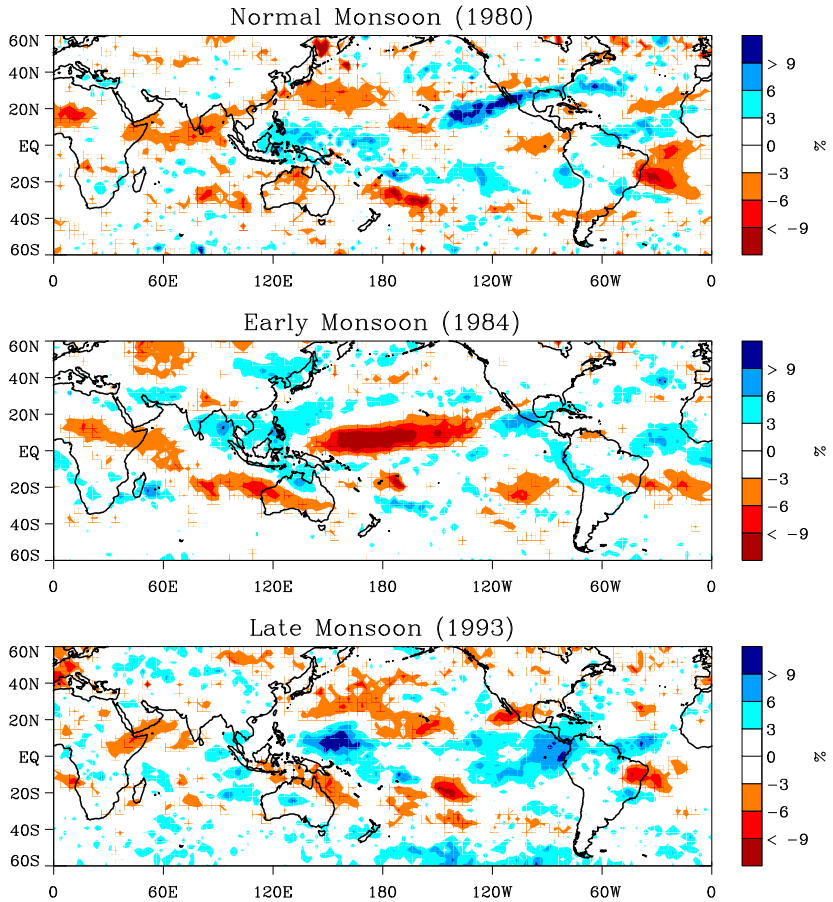

Fig. 5.6. Monthly mean interannual anomalies of upper tropospheric humidity for March preceding normal, early, and late onset of the South China Sea monsoon.

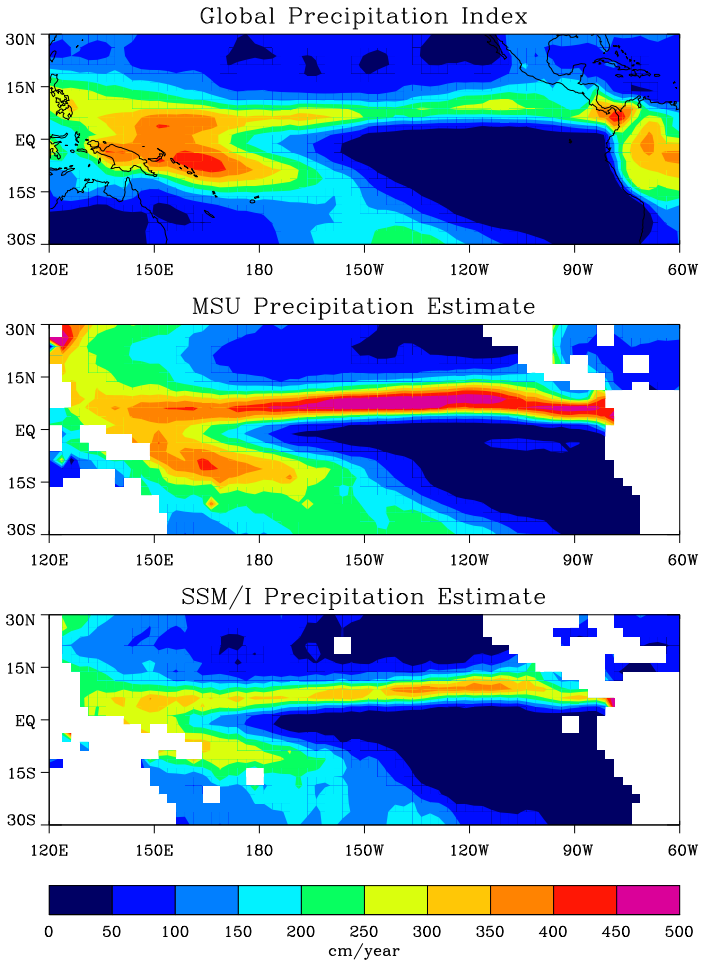

Fig. 5.7. Average annual rainfall estimated from three different satellite sources. The top image was created from geostationary infrared data using Arkin and Meisner's (1987) GPI technique, the middle image is from microwave sounding unit (MSU) estimates produced by Spencer (1993), and the bottom image is from SSMI estimates by Berg and Chase (1992).

lite estimates validated over the west Pacific will tend to underestimate the total rainfall in the east Pacific by almost a factor of three. This finding is consistent with the rainfall estimates shown in **Fig. 5.7**. The use of multispectral satellite imagery is currently being investigated to help quantify and explain this fundamental difference between precipitating systems in the two regions. A combination of satellite rainfall and water vapor estimates from both polar orbiting and geostationary platforms is being used to investigate low-level moisture transport converging into the ITCZ, and the subsidence and drying of the upper troposphere above the ITCZ. These processes are unique to the east Pacific ITCZ and give rise to the large discrepancies in estimates of precipitation and hence latent heat release and the resultant seasonal to interannual circulation anomalies.

Investigations of upper tropospheric brightness temperature anomalies from the SSMT2 moisture sounder on board the DMSP satellites have shown the presence of intraseasonal variability in this water vapor signal which is not apparent in OLR observations (Berg, 1996). Band pass filtered brightness temperature anomalies from the SSMT2 183 ± 1 GHz channel are shown for the equatorial belt in **Fig. 5.8**. The brightness temperatures from this channel are sensitive to water vapor above ~500mb as well as both liquid water and ice, making it particularly useful for hydrological studies. Moisture increases in any water phase result in a decrease in the associated brightness temperatures. As a result, this combined phase moisture signature can be used to identify and track features much better than the OLR anomalies shown in the left panel of **Fig. 5.8**. The SSMT2 anomalies shown in the right panel of **Fig. 5.8** indicate the same eastward propagating MJO signature as the OLR, but a westward propagating signal of the opposite phase is also present in the SSMT2 anomalies, resulting in a cancellation over the east Pacific.

5.5. Studies of air-sea interactions

5.5.1. Wind speed and direction from passive and active microwave observations

We have been analyzing passive microwave data from the SSMI and scatterometer data from the ERS-1 so these data can be optimally used for estimating the air-sea heat and momentum

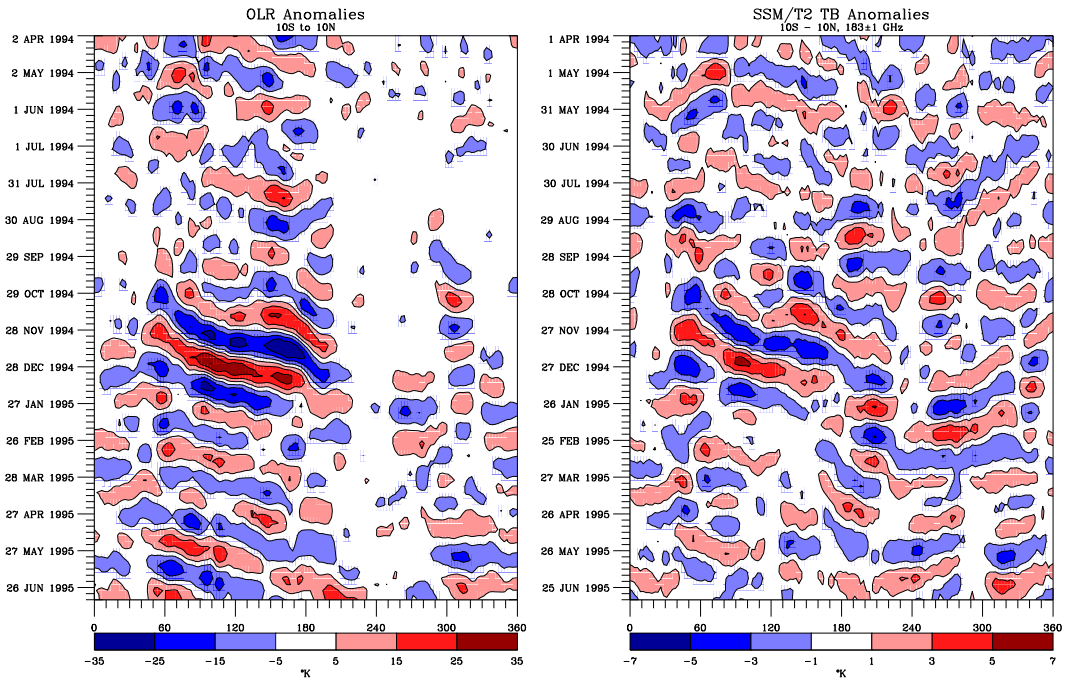

Fig. 5.8. Zonally averaged anomalies of a) OLR and b) 183 ± 1 GHz (upper troposphere) SSMT2 brightness temperatures with a 35 to 90 day band pass filter applied.

fluxes. Recent observational results from aircraft suggest there is a detectable wind direction signal in passive microwave data. The action of the surface wind upon the ocean surface wave spectrum may be thought of in terms of a two-scale model; the longwave scale is related to the large-scale slope distribution of the ocean gravity waves and the shortwave scale related to the small scale distribution of the capillary waves. The wind direction signal in passive microwave data is thought to originate from a resonant emission phenomena due to the small scale capillary wave distribution. **Fig. 5.9** shows the theoretical change in brightness temperature as a function of wind speed and direction for the 37 Ghz vertical polarization for near nadir viewing angles. In reality, however, the SSMI observes the ocean surface at a 53˚ incidence angle, so this resonance wind direction signal is masked by an additional signal due to the slopes of the large waves. We are using buoy data from NDBC and the TOGA-TAO moorings matched with SSM./I observations to assess the practical application of this technique (Bates and McColl, 1995).

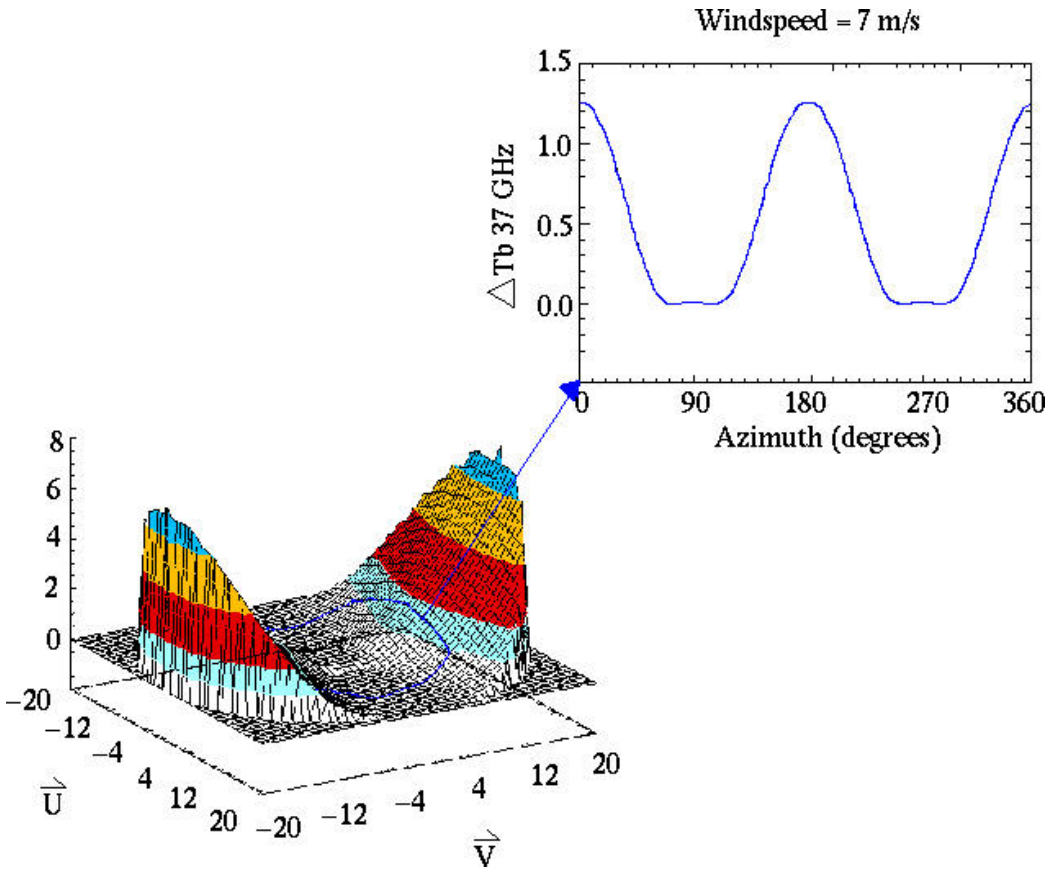

Fig. 5.9. Simulated increase in passive microwave brightness temperature as a function of wind speed and direction for 37 Ghz vertical polarization.

5.5.2. Satellite radar observations of the ocean surface

Both active and passive microwave techniques can be used to retrieve estimates of ocean winds speed and direction, but the understanding of what processes contribute to the observed signals requires high resolution data sets, such as provided by SAR, and field experiments such as the coastal ocean probing experiment (COPE). We are conducting collaborative work with NOAA Environmental Technology Laboratory in radar observations of the ocean surface. We have completed a major technical memorandum on the analysis of the Russian Almaz synthetic aperture radar (SAR) observations of ocean surface phenomena (Bates and Gottschall, 1996). Prior research has shown that HH polarized microwave backscatter is very different from VV polarized backscatter when ocean waves break. Under these circumstances, the spectrum of the HH polarized backscatter shifts to higher frequencies and the spectral width (second moment) becomes broader. We are analyzing wave tank, COPE field data, and Almaz SAR data to examine whether the doppler spectral width can be used to characterize breaking wave action on the ocean surface. This type of data, in turn, may be used to improve our understanding of the ocean surface wave spectrum and remote sensing observations of ocean surface winds and fluxes.

5.5.3. Sea surface temperature

Sea surface temperatures are used as the primary boundary condition for most seasonal to interannual forecasting schemes. Thus, accurate global observations of SST are critical for improving these forecasts. NOAA NESDIS has been producing estimates of SST using high resolution multispectral infrared data from the NOAA polar-orbiting satellites for over 10 years. However, the utility of this data set for climate and global change studies remains only marginal because of large biases during volcanic aerosol episodes and operational constraints. Bates (1994) critically examined the first 10 years of this satellite-derived SST product with respect to three criteria: 1) the basic physics of the method, 2) mean differences between satellite derived and in-situ SSTs, and 3) the space/time variability of the data set.

Fig. 5.10 shows the zonally-averaged difference between the satellite derived SST analysis and COADS. During this 10-year period, two major bias events, due to stratospheric aerosols, are evident. The first event occurs in the Spring of 1982 and is associated with the eruption of El Chichon. The maximum anomaly is approximately -2˚C soon after the eruption. The biases expanded with time in latitude and biases of -1˚C remain throughout 1983. In late Spring 1991, a series of eruptions occurred on Mt. Pinatubo. Biases immediately after the eruption exceeded - 5˚C. In late summer 1991, NESDIS implemented a new algorithm in an attempt to correct for the volcanic aerosols. Some decrease in the biases are evident from this change, but smaller persistent negative biases are still evident in the tropics. We are working with R. Reynolds of the NOAA Coupled Model Project to improve our understanding of the satellite derived SST product and blend these data with in-situ observations to obtain the best possible SST product.

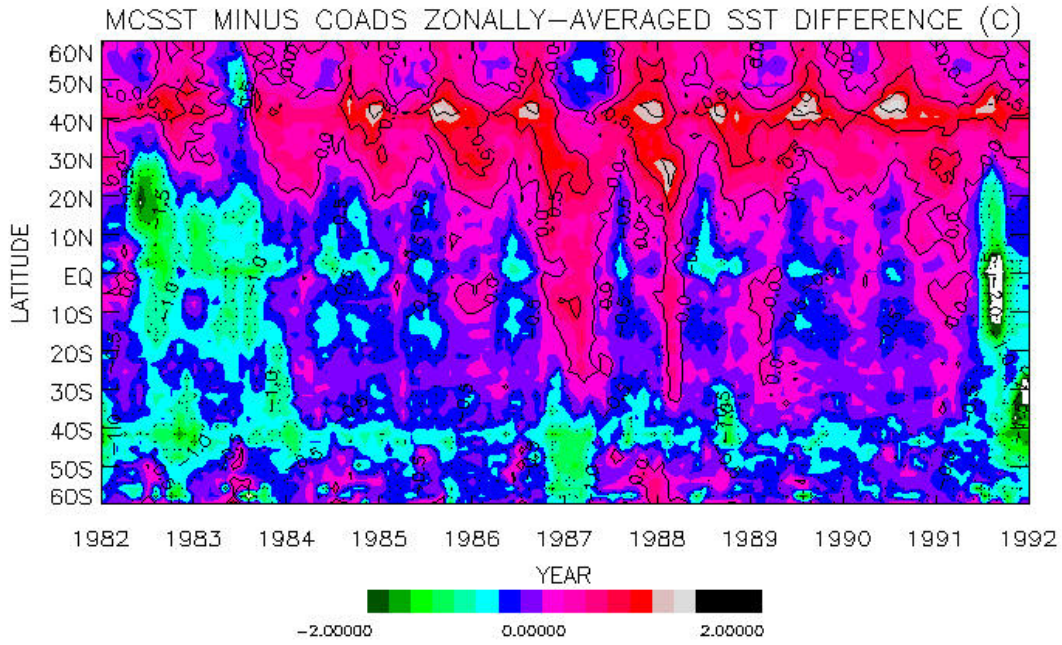

Fig. 5.10. Zonally averaged mean monthly difference (˚C) between MCSST analysis and the COADS SST data.

Contributed by: *J. Bates, W. Berg, Q. Ye, and D. Jackson.*

References:

Journal Articles

Bates, J. J., H. F. Diaz, R. W. Reynolds and R. L. Bernstein 1993: Using satellite infrared data in studies of variabilities of the Western Pacific warm pool. *Science*, **262**,440-441.

Bates, J. J. 1994: A decade of multispectral sea surface temperature observations from space. *Adv. in Space Res.*, **14**,(3)5-(3)14.

Bates, J. J., X. Wu and D. L. Jackson 1996: Interannual variability of upper troposphere water vapor band brightness temperature. *J. Climate*, **9**,427-438.

Berg, W. and S. K. Avery 1994: Rainfall variability over the tropical Pacific from July 1987 through December 1991 as inferred via monthly estimates from SSM/I. *J. Appl. Meteor.*, **33**,1468-1485.

Berg, W. and S. K. Avery 1995: An evaluation of monthly rainfall estimates derived from SSM/I over the tropical Pacific. *J. Geophys. Res.*, **100**,1295-1315.

Berg, W. and R. Chase, 1992: Determination of mean rainfall from the Special Sensor Microwave/Imager (SSM/I) using a mixed lognormal distribution, *J. Atmos. Oceanic Technol.*, **9**, 129-141.

Deser, C., J. J. Bates and S. Wahl 1993: The influence of sea surface temperature on stratiform cloudiness along the equatorial front in the Pacific Ocean. *J. Climate*, **6**,1172-1180.

Emery, W. J., Y. Yu, G. A. Wick, P. Schluessel and R. W. Reynolds 1994: Correcting infrared satellite estimates of sea surface temperature for atmospheric water vapor attenuation. *J. Geophys. Res.*, **99**,5219-5236.

Greenwald, T. J., G. L. Stephens, T. H. V. Haar and D. L. Jackson 1993: A physical retrieval of cloud liquid water over the global oceans using SSM/I observations. *J. Geophys. Res.*, **98**,18471-18488.

Jackson, D. L. and G. L. Stephens 1995: A study of SSM/I derived columnar water vapor over the global oceans. *J. Climate*, **8**,2025-2038.

Privette, J. L., C. Fowler, G. A. Wick, D. Baldwin and W. J. Emery 1995: Effects of orbital drift on advanced very high resolution radiometer products: Normalized difference vegetation index and sea surface temperature. *Remote Sens. Environ.*, **53**,164-171.

Stephens, G. L., D. L. Jackson and J. J. Bates 1994: A comparison of SSM/I and TOVS column water vapor data over the global oceans. *Meteorol. Atmos. Phys.*, **54**,183-201.

Stephens, G. L., D. L. Jackson and I. Wittmeyer 1996: Global observations of upper-tropospheric water vapor derived from TOVS radiance data. *J. Climate*, **9**,305-326.

Sun, G. and Q. Ye 1996: A study on the variation of drought periods occurring in northwest China and other Africa-Asia contiental regions. *Acta Meteorologica Sinica*, **10**,473-484.

Wu, X., J. J. Bates and S. J. S. Khalsa 1993: A climatology of water vapor band brightness temperatures from the NOAA operational satellites. *J. Climate*, **6**,1282-1300.

Ye, Q. and J. J. A. Coakley 1996: Biases in Earth Radiation Budget Observations, Part I: Effects of Scanner Spatial Resolution on the Observed Anisotropy. *J. of Geophy. Res.*, **101(D16)**,21243-21252 .

Ye, Q. and J. J. A. Coakley 1996: Biases in Earth Radiation Budget Observations, Part II: Consistent Scene Identification and Anisotropy Factors. *J. of Geophy. Res.* , **101(D16)**,21253-21264.

Ye, Q. and A. Xie 1996: Summer Monsoon Onset and Its Interannual Variability in the South China Sea. *Acta Meteorologica Sinica*, **54**,72-80 (in Chinese) .

Ye, Q., A. Xie and Y. J. Zhu 1996: Climatological Background Study for the HUBEX Based on Multichannel Satellite Observatoins. *Acta Meteorologica Sinica*, **54**,252-264 (in Chinese) .

Book Sections

Ye, Q. 1995: Some Climatical Characters of Summer Monsoon Onset in the South China Sea . *1995 Pan-Pacific Science*, 12-17 Jun.

Submitted or in Press

Bates, J. J. and D. L. Jackson 1997: A comparison of water vapor observations with AMIP-I simulations. *J. Geophys Res.*, **submitted**.

Berg, W., W. Olson, R. R. Ferraro, S. J. Goodman and F. J. LaFontaine 1996: An assessment of the first and second generation Navy operational precipitation retrieval algorithms. *J. Atmos. Sci.*, **accepted**.

Ferraro, R. R., E. A. Smith, W. Berg and G. J. Huffman 1996: A review of screening techniques for passive microwave precipitation retrieval algorithms. *J. Atmos. Sci.*, **accepted**

Ye, Q. and A. Xie 1997: A climatological study of summer monsoon onset in the South China Sea. *J. Climate*, **submitted**.

Ye, Q., A. Xie, and X. Liu, 1997: On the Impact of the Equatorial Westerly Winds in the Indian Impact on the South China Sea Monsoon Onset, *J. Meteor. Soc. Japan*, **submitted**

Conference Proceedings and other Gray Literature

Bates, J. J., and C. C. Gottschall, 1996: Analysis of Almaz SAR ocean imagery. Technical Memorandum prepared for the Department of Defense Advanced Sensor Applications Program.

Bates, J. J., and K. C. McColl, 1995: Observational and theoretical evidence for a wind vector signal in SSMI data. Presented at IAPSO XXI General Assembly, Honolulu, Hawaii.

Berg, W., 1994: Precipitation retrieval during TOGA COARE using a combination of SSM/I and GMS data with application to climate studies, in *Proceedings of the seventh conference on satellite meteorology and oceanography,* June 6-10, Monterey, CA, 67-70.

Berg, W., 1996: An analysis of moisture variability in the eastern tropical Pacific using SSMT2 data, in *Proceedings of the eighth conference on satellite meteorology and oceanography,*